



## Studying the Effect of Adding a Buffer Layer and Back Reflection on the Performance of Chalcogenide Practically and by Simulation

Hardan T. Ghanem

Ministry of Education, Directorate of Education, Salah Al-Din Governorate

**Keywords:** Chalcogenide compounds, SCAPS-D, Layer BSL, Layer Buffer, simulation.

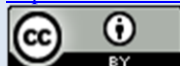
### ARTICLE INFO.

#### Article history:

-Received: 23 July 2023  
-Received in revised form: 17 Sep. 2023  
-Accepted: 20 Sep. 2023  
-Final Proofreading: 24 Oct. 2023  
-Available online: 25 Oct. 2023

**Corresponding Author\*:**  
Hardan T. Ghanem

© THIS IS AN OPEN ACCESS ARTICLE UNDER THE CC BY LICENSE  
<http://creativecommons.org/licenses/by/4.0/>



### ABSTRACT

Solar energy is one of the most important methods used worldwide to provide some of the global energy requirements. It is easily available and free from negative effects on the environment. In this research, the possibility of increasing the efficiency of solar cells is investigated. The SCAPS-D simulation is used to investigate the ZnO/ZnS/CNTS solar cell. The practical research is compared with the program, showing that the program simulates the reality due to the high convergence between the practical and theoretical results of the program. By changing the doping ratios of the theoretical cell layers, the cell efficiency shifts from (3.19%) to (9.41%). The theoretical cell is improved by adding various back reflection layers (BSL), increasing the conversion efficiency from (9.41%) to (11.59%). After adding more matching layers, the cell's structure becomes ZnO/ZnS/V<sub>2</sub>O<sub>5</sub>/CNTS, increasing the conversion efficiency to (14.25%). The ratio of conversion efficiency of ZnS/V<sub>2</sub>O<sub>5</sub>/CNTS/CFTS is (17.22%), the filling factor (67.74%), the short circuit current (23.247mA/cm<sup>2</sup>), and the open circuit voltage (1.0937 V).

## دراسة تأثير إضافة طبقة موائمة وانعكاس خلفي على أداء الكالوجينيد عملياً وعن طريق المحاكاة

حردان ذياب غانم

وزارة التربية مديرية تربية صلاح الدين

## المخلص

تعتبر الطاقة الشمسية من أهم الطرق المتبعة عالمياً لتوفير بعض متطلبات الطاقة العالمية، وهي متوفرة بسهولة وخالية من التأثيرات السلبية على البيئة. درست الخلية الشمسية ZnO/ZnS/CNTS باستخدام محاكاة برنامج SCAPS-D. وقورنه البحث العملي مع البرنامج وتبين من الدراسة ان البرنامج يحاكي الواقع بسبب التقارب الكبير بين النتائج العملية و النتائج النظرية للبرنامج , وبتغيير نسب التشويب لطبقات الخلية النظرية تحولت كفاءة الخلية من (3.19%) الى (9.41%) ثم تم تحسين الخلية النظرية بإضافة مختلف طبقات الانعكاس الخلفي (BSL) فزادت كفاءة التحويل من 9.41% الى 11.59%, واضيفت عدت طبقات موائمة فاصبح شكل الخلية ZnO/ZnS/V<sub>2</sub>O<sub>5</sub>/CNTS وتحولت كفاءة التحويل الى (14.25%) فيتبين ان تأثير طبقة الموائمة اكبر من طبقة الانعكاس واخيرا ادخلت افضل طبقة موائمة (V<sub>2</sub>O<sub>5</sub>) مع مختلف طبقات الانعكاس وتبين ان افضل خلية شمسية ZnO/ZnS/V<sub>2</sub>O<sub>5</sub>/CNTS/CFTS بكفاءة تحويل (17.22%) وعامل المليء (67.74%) وتيار الدائرة القصيرة (23.247mA/cm<sup>2</sup>) وفولتية الدائرة المفتوحة (1.0937 V).

## 1. Introduction

Semiconductors capture photons with energies over the limited energy gap and release the surplus energy through thermal, radiative, or non-radiative processes. Efforts are being made to improve the semiconductor efficiency by producing different types of solar cells [1]. Since these materials are known for their high efficiency, researchers have been drawn to use the compounds of Copper Indium Gallium Selenide (CIGS) and Cadmium telluride (CdTe) in the production of thin films for solar cells for several decades. An alternate substance with good electrical and optical characteristics that is readily accessible and non-toxic would be Copper, zinc, tin, and sulfur CuZnSnS<sub>4</sub> (CZTS). New compounds can be investigated by substituting (Zn) with (Ni, Fe, Cd, Be, Mg, Mn) and other elements. It is known as quaternary chalcogenide, is found in the Earth's crust, is synthesized at a reasonable cost, is non-toxic, has a bandgap energy that is near the ideal value, and has a high absorption coefficient [2,3]. Because of their excellent optical and electrical qualities for the production of thin films, interest in these materials has grown.

The substance CuNiSnS<sub>4</sub> (CNTS) is one of the significant compounds due to its unique properties, including its proximity to

the ideal direct energy gap (1.45eV-1.74eV), availability in the earth's crust, non-toxicity, p-type, high absorption coefficient, and capacity to absorb the entire spectrum. The compound is a potential compound for producing solar cells since it can be manufactured using spin coating, dip coating, and other techniques [4-7]. In 2020, Beraich manufactured the CNTS thin films with a quadruple structure, and the SEM image showed that these films were homogeneous and their energy gap was within (1.6 eV-1.8 eV) [8]. This study will investigate (CNTS) as an absorption layer, compare the results from experiments with those from simulations, and investigate whether adding a back-reflection layer and a buffer layer, adjusting the concentration of donors and receptors, adjusting the thickness, and other factors, could improve the characteristics of cells. Therefore, CNTS can be considered a candidate material to be used as photovoltaic cells.

## 2. Modeling

## 2.1. Numerical Simulations in SCAPS

The University of Ghent in Belgium has developed the solar cell capacitance simulator (SCAPS) program (version 3.3.07 (SCAPS3307), which is compatible with Windows 95, 98, NT, 2000, XP, Vista, and Windows 7), a one-dimensional solar

cell modeling tool, to simulate the standard semiconductor crystalline materials like CIGS, CdTe, or alternative materials like SnS. When describing a cell's many characteristics, such as optical absorption, thickness, doping concentration, energy gap, etc., the user is limited to describing a cell with a maximum of seven layers. In both the light and the dark environments, the spectral responses may be computed as a function of temperature. All solar cells are subjected to this program's development. It is an application that is free to use. It depends on resolving equations involving semiconductors. The Poisson equation is first written by [9] as:

$$\nabla(E) = \frac{q}{\epsilon} (p - n + N_D^+ - N_A^-) \quad (1)$$

Where E is the electrical field, q is the elementary charge, ε is the permittivity of the absorber, n(p) is the density of electrons (holes), and N<sub>D</sub> (N<sub>A</sub>) is the donor (acceptor) concentration.

As a result, the following connection provides the continuity equation [10]:

$$\frac{dn}{dt} = \frac{1}{q} (\nabla(J_n) + G_n - R_n) \quad (2)$$

$$\frac{dp}{dt} = - \frac{1}{q} (\nabla(J_p) + G_p - R_p) \quad (3)$$

Where J<sub>n</sub> (J<sub>p</sub>) is the electron (hole) current density, G<sub>n</sub> (G<sub>p</sub>) is the electron (hole) generation rate and R<sub>n</sub> (R<sub>p</sub>) is the electron (hole) recombination rate.

The following equations can be used to get the charge carrier equations for the diffusion and drift current densities [11]:

$$J_n = q(\mu_n nE + D_n \nabla n) \quad (4)$$

$$J_p = q(\mu_p pE + D_p \nabla p) \quad (5)$$

Where μ<sub>n</sub> (μ<sub>p</sub>) is the Electron (hole) mobility and D is the diffusion constant.

The filling factor (FF), the short circuit current (J<sub>sc</sub>), the open circuit voltage (V<sub>oc</sub>), and the conversion efficiency must all be known to assess the quality of photovoltaic

cells since these variables are connected by the following equations [11]:

$$FF = \frac{P_{max}}{P_t} = \frac{V_{max} . I_{max}}{V_{oc} . J_{sc}} \quad (6)$$

$$\eta = \frac{P_m}{P_{in}} = \frac{V_{oc} . J_{sc} . FF}{P_{in}} \quad (7)$$

Where V<sub>max</sub> is the Voltage greatest, P<sub>max</sub> is the power greatest, I<sub>max</sub> is the current greatest, and P<sub>in</sub> is the Incoming power.

The following link between the concentration of doping and recombination and the age of minority carriers, which is the average amount of time needed for their recombination, may be used to estimate the age of minority carriers [12].

$$\tau = \frac{1}{\sigma V_{th} N_t} \quad (8)$$

$$\tau = \frac{\Delta n}{U} \quad (9)$$

Where τ is the minority carrier lifetime, N<sub>t</sub> is the defects concentration, V<sub>th</sub> is the Thermal speed, σ is the Conductivity, U is the recombination rate and Δn is the excess minority carrier concentration.

## 2.2. The Structure of the Solar Cell

The CNTS/ZnS/ZnO solar cell is made up of three layers: a Zinc Oxide (ZnO) window layer of transparent metal oxides with a relatively large energy gap; a buffer Zinc sulfide (ZnS) layer with an energy gap suitable for the absorption layer gradient with penetration; and finally, the CNTS absorption layer with a relatively small energy gap. It also has front and back contacts made of aluminum and gold with functional working contacts (5 eV and 4.1 eV, respectively). The cell is on a floor of glass [13]. Tables (1) and (2) provide the values for the program parameters and faults, respectively, that must be taken into account in the SCAPS program's absorption layer to analyze the performance of the

experimental cell. The installation of the solar cell is shown in Figure 1.

AL )front)
ZnO Window Layer
buffer Layer ZnS
absorption Layer CNTS
(back) Au
glass

**Figure 1:** The installation of the solar cell

The following issues need to be resolved if solar cells are to become more efficient:

- Comparing the theoretical cell to the experimental cell.
- Increasing the cell efficiency by adding multiple back reflection layers.
- Adding additional layers of alignment to enhance cell performance.
- Combining the best alignment and reflection layers for creating the ideal cell.

**Table 1:** The physical parameters of different layers [14-19]

Parameters	symbol (unit)	CNTS	ZnS	ZnO
Thickness	W( $\mu\text{m}$ )	3.1	0.09	0.9
Bandgap	Eg (ev)	1.74	3.18	3.22
Electron affinity	$\chi$ (ev)	3.87	4.5	4.4
Dielectric permittivity	$\epsilon_r$	9	10	9
CB effective density of states	$N_C(\text{cm}^{-3})$	$2.2 \times 10^{18}$	$1.8 \times 10^{18}$	$2.2 \times 10^{18}$
VB effective density of states	$N_V(\text{cm}^{-3})$	$1.8 \times 10^{19}$	$1.8 \times 10^{19}$	$1.8 \times 10^{19}$
Electron thermal velocity	$V_n(\text{cm/s})$	$1.0 \times 10^7$	$1.0 \times 10^7$	$1.0 \times 10^7$
Hole thermal velocity	$V_p(\text{cm/s})$	$1.0 \times 10^7$	$1.0 \times 10^7$	$1.0 \times 10^7$
Electron mobility	$\mu_n(\text{cm}^2/\text{v.s})$	11	100	100
Hole mobility	$\mu_p(\text{cm}^2/\text{v.s})$	11	25	25
Shallow uniform donor density	$N_D(1/\text{cm}^3)$	0	$1.0 \times 10^{16}$	$1.0 \times 10^{19}$
Shallow uniform acceptor density	$N_A(1/\text{cm}^3)$	$3.3 \times 10^{17}$	0	0
Coefficient absorption	$\alpha(1/\text{cm})$	$5.0 \times 10^4$	$1.0 \times 10^5$	scaps

**Table 2:** the defect value in the cell

Defect properties	Interface defect p-CNTS/n-ZnS	Absorber layer p-CNTS
Energy level with respect to reference (eV)	0.6	0.6
Total density Nt ( $\text{cm}^{-2}$ )	$1.0 \times 10^{11}$	$1.0 \times 10^{15}$
Capture cross section area of electrons ( $\text{cm}^2$ ) $\delta_e$	$1.0 \times 10^{-15}$	$1.0 \times 10^{-15}$

### 3. Discussion of Findings

#### 3.1. Comparing the Experimental Cell to the Theory

To simulate the performance of a solar cell, the program utilized must be validated and its consistency with real findings must

be demonstrated. The practical research of Ghosh, Anima, et al. [15] is simulated on the SCAPS program. The results show a high level of agreement between the practical and theoretical results, as shown in Table (3), but with an incomplete

congruence of the two curves' properties (V-I). The results shown in Figure (2) demonstrate a drop in the filling factor, leading to a fall in the conversion efficiency. This is attributed to the flaws in the p-CNTS/n-ZnS interface and the p-CNTS absorption layer. When the number of  $N_t$  faults decreases, the experimental

work equals the theoretical work. Because of the rise in the permanence of minority carriers, which is inversely proportional to the defects, as indicated in equation (8), the recombination will decrease, and the theoretical cell efficiency will increase over the experimental cell, as shown in equation (9).

**Table 3:** the theoretical and experimental results

Solar cell	V (v)	J(mA/cm <sup>2</sup> )	FF %	% $\eta$
CNTS/ZnS/ZnO (Experimental) [15]	0.75	6.82	53.1	2.71
CNTS/ZnS/ZnO (Theoretical)	0.73	6.74	64.26	3.19

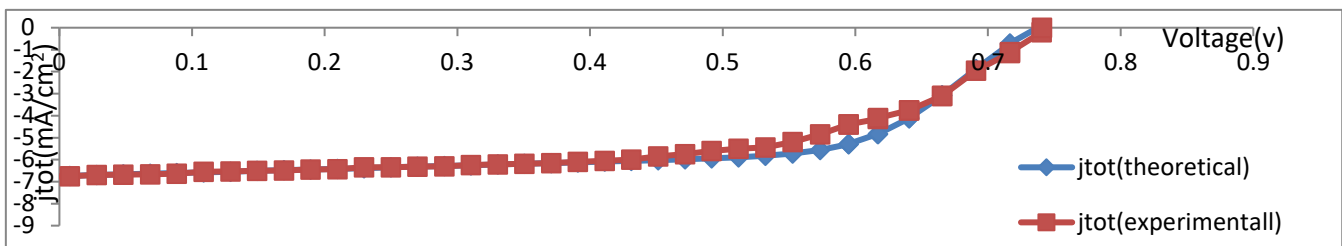


**Figure 2:** Voltage-current relationships for experimental and theoretical curves

**Table 4:** Outputs for experimental, theoretical, and improved cells

Cells	V(v)	J(mA/cm <sup>2</sup> )	FF%	$\eta$ %
ZnO/ZnS/CNTS (Theoretical)	0.7359	6.743	64.26	3.19
ZnO/ZnS/CNTS (After Optimization)	0.934	16.749	60.11	9.41

### 3.2.The Effect of Back Reflection Layer

To enhance the investigated cell ZnO/ZnS/CNTS, this study investigates the effect of adding different back reflection layers (BSL) composed of the following chemicals ( MoSe<sub>2</sub>, SnS, CdTe, Si, ZnTe, Cu<sub>2</sub>O, CuO, CuSbS<sub>2</sub>, MoS<sub>2</sub>, CuInSe (CISe), CuInGaS<sub>4</sub> (CIGS), CZTS, CZTSe, CuFeSnS<sub>4</sub> (CFTS), CNTS, CuBaSnS<sub>4</sub> (CBTS), MASnI<sub>3</sub>, CZTSSe, Cu<sub>2</sub>Te). The sole difference in the enhanced cell with the stability of the cell characteristics is the thickness and doping concentration of the back-reflection layer. The parameters of the back-reflection layers are shown in Table

(5). In contrast to photons entering from the absorption layer, which increases charge carrier concentration and minimizes recombination, the connection becomes more ohmic, and the photon's current increases [21]. The best back reflection layers are (Cu<sub>2</sub>O, CBTS, and CZTSe) for two reasons: firstly, the total of the energy gap and the electronic affinity equals or exceeds the work function. Secondly, because of the large potential barrier, the quantity of photons reflected from the rear surface increases [12]. The results of adding different back reflection layers are clarified in table 6.

**Table 5:** the basic parameters of back reflection layer [22-31]

Parameters symbol (unit)	MoSe <sub>2</sub>	SnS	CdTe	Si	ZnTe	Cu <sub>2</sub> O	CuO	CuS bS <sub>2</sub>	MoS <sub>2</sub>	ClSe	CIGS
Bandgap E <sub>g</sub> (ev)	1.060	1.1-1.3	1.4-1.9	1.12	2.19	2.17	1.51	1.5	1.7	1	1.05
Electron affinity χ (ev)	4.372	12.5	4.28	4.05	3.73	3.2	4.07	4.5	4.2	4.5	4.14
Dielectric permittivity ε/ε <sub>r</sub>	13.6	4.2	9.4	11.9	10.3	7.11	18.1	10	13.6	13.6	10
CB effective density of states N <sub>C</sub> (cm <sup>-3</sup> ) × 10 <sup>18</sup>	2.2	10.0	0.75	25.8	1.17	0.20	22	2.0	2.2	2.2	1.0
VB effective density of states N <sub>V</sub> (cm <sup>-3</sup> ) × 10 <sup>19</sup>	1.8	4.13	1.8	2.65	1.166	1.1	55.0	1.0	1.8	1.8	1.0
Electron thermal velocity V <sub>n</sub> (cm/s) × 10 <sup>7</sup>	1.0	1.0	1.0	1.0	1.0	1.0	1.0	1.0	1.0	1.0	1.0
Hole thermal velocity V <sub>p</sub> (cm/s) × 10 <sup>7</sup>	1.0	1.0	1.0	1.0	1.0	1.0	1.0	1.0	1.0	1.0	1.0
Electron mobility μ <sub>n</sub> (cm <sup>2</sup> /v.s)	100	25	500	1350	330	200	100	100	100	40	30
Hole mobility μ <sub>p</sub> (cm <sup>2</sup> /v.s)	25	100	60	450	80	80	0.1	25	25	10	15
Shallow uniform donor density N <sub>D</sub> (1/cm <sup>3</sup> )	0	0	0	0	0	0	0	0	0	0	0
Shallow uniform acceptor density N <sub>A</sub> (1/cm <sup>3</sup> ) × 10 <sup>18</sup>	0.001	10000	1000	10000	100	10	10000	100	100	100	10000

**Complement of Table 5**[16,18,19,32-35]

Parameterssymbol (unit)	CZTS	CZTSe	CFTS	CNTS	CBTS	MASnI <sub>3</sub>	CZTSSe	Cu <sub>2</sub> Te
Bandgap E <sub>g</sub> (ev)	1.4	1.4	1.3	1.74	1.9	1.3	1.3	1.18
Electron affinity χ (ev)	4.5	4.1	3.3	3.87	3.6	4.17	4.2	4.2
Dielectric permittivity ε/ε <sub>r</sub>	9	9	9	9	5.4	8.2	13.6	10
CB effective density of states N <sub>C</sub> (cm <sup>-3</sup> ) × 10 <sup>18</sup>	2.2	22	2.2	2.2	2.2	2.8	2.2	0.78
VB effective density of states N <sub>V</sub> (cm <sup>-3</sup> ) × 10 <sup>19</sup>	1.8	0.18	1.8	1.8	1.8	0.39	1.8	1.6
Electron thermal velocity V <sub>n</sub> (cm/s) × 10 <sup>7</sup>	1.0	1.0	1.0	1.0	1.0	1.0	1.0	1.0
Hole thermal velocity V <sub>p</sub> (cm/s) × 10 <sup>7</sup>	1.0	1.0	1.0	1.0	1.0	1.0	1.0	1.0
Electron mobility μ <sub>n</sub> (cm <sup>2</sup> /v.s)	60	100	11, 98	11	30	0.16	100	500
Hole mobility μ <sub>p</sub> (cm <sup>2</sup> /v.s)	20	12.5	11, 98	11	10	0.16	25	100
Shallow uniform donor density N <sub>D</sub> (1/cm <sup>3</sup> )	0	0	0	0	0	0	0	0
Shallow uniform acceptor density N <sub>A</sub> (1/cm <sup>3</sup> ) × 10 <sup>20</sup>	1.0	100	100	0.0033	1.0	100	100	100

**Table 6:** the results of adding different back reflection layers

	cells	V(v)	J(mA/cm <sup>2</sup> )	FF%	η %
1.	ZnO/ZnS/CNTS ( Theoretical)	0.7359	6.743	64.26	3.19
2.	ZnO/ZnS/CNTS (After Optimization)	0.934	16.749	60.11	9.41
3.	ZnO/ZnS/CNTS/MoSe <sub>2</sub>	1.01	16.759	57.66	9.76
4.	ZnO/ZnS/CNTS/SnS	1.103	16.867	61.54	11.46
5.	ZnO/ZnS/CNTS/CdTe	0.89	16.9	60.18	9.05
6.	ZnO/ZnS/CNTS/Si	1.1	16.83	61.56	11.43
7.	ZnO/ZnS/CNTS/ZnTe	1.059	17.0	62.05	11.18
8.	<b><u>ZnO/ZnS/CNTS/Cu<sub>2</sub>O</u></b>	<b><u>1.106</u></b>	<b><u>17.03</u></b>	<b><u>61.5</u></b>	<b><u>11.59</u></b>
9.	ZnO/ZnS/CNTS/CuO	1.091	16.81	61.7	11.44
10.	ZnO/ZnS/CNTS/CuSdS <sub>2</sub>	0.648	16.734	51.07	5.54
11.	ZnO/ZnS/CNTS/MoS <sub>2</sub>	0.763	16.8	53.16	6.82
12.	ZnO/ZnS/CNTS/CISE	2.69	16.89	24.32	11.06
13.	ZnO/ZnS/CNTS/CIGS	1.1	16.843	61.55	11.44
14.	ZnO/ZnS/CNTS/CZTS	0.736	16.808	54.83	6.796
15.	<b><u>ZnO/ZnS/CNTS/CZTSe</u></b>	<b><u>1.098</u></b>	<b><u>16.985</u></b>	<b><u>61.63</u></b>	<b><u>11.50</u></b>
16.	ZnO/ZnS/CNTS/CFTS	0.959	17.275	41.79	6.93
17.	ZnO/ZnS/CNTS/CNTS	1.02	16.96	61.91	10.74
18.	<b><u>ZnO/ZnS/CNTS/CBTS</u></b>	<b><u>1.099</u></b>	<b><u>17.025</u></b>	<b><u>61.59</u></b>	<b><u>11.53</u></b>
19.	ZnO/ZnS/CNTS/MASnI <sub>3</sub>	1.086	16.989	61.84	11.41
20.	ZnO/ZnS/CNTS/CZTSSe	1.083	16.983	61.82	11.38
21.	ZnO/ZnS/CNTS/Cu <sub>2</sub> Te	1.104	16.901	61.54	11.48

### 3.3.The Effect of Adaptation Layer (CuNiSnS<sub>4</sub>)

Various buffer layers are also added to the ZnO/ZnS/CNTS cell with the cell parameters fixed, so the change will only be in the matching layer in terms of layer type, thickness, and concentration of impurities. The matching layer increases the access of photons to the absorption layer due to its reduction of surface defects. Between the penetration and absorption layers [36], it is found that it has a significant effect on the cell parameters and that its effect is greater than the effect of the back reflection layer (BSL) due to the large difference in the energy gap between the absorption layer and the permeable layer, and the compounds consist of materials (TiO<sub>2</sub>, CdS, In<sub>2</sub>S<sub>3</sub>, ZnO:Al, V<sub>2</sub>O<sub>5</sub>, SiC). The best matching layers are (TiO<sub>2</sub>, and V<sub>2</sub>O<sub>5</sub>) because TiO<sub>2</sub> has a high energy gap, allowing the most photons to enter into the absorption layer, but V<sub>2</sub>O<sub>5</sub> has very little mobility, resulting in an increase in the electric field and an increase in the number of absorbed photons. The fundamental parameters are shown in Table (7). Table (8) illustrates the results achieved by adding an adaptive layer to the enhanced cell, with the cell composition of CNTS /Buffer/ ZnO/ZnS.

**Table 7:** the basic parameters of buffer layer [14,26,29,33,35,37]

Parameters	symbol (unit)	TiO <sub>2</sub>	CdS	In <sub>2</sub> S <sub>3</sub>	ZnTe	V <sub>2</sub> O <sub>5</sub>	SiC
Bandgap	E <sub>g</sub> (ev)	3.2	2.4	2.8	2.19	2.3	2.3
Electron affinity	χ (ev)	3.86	4.5	4.7	3.73	3.99	3.8
Dielectric permittivity	ε/ε <sub>r</sub>	9	9	13.5	10.3	4.28	9.72
CB effective density of states	N <sub>C</sub> (cm <sup>-3</sup> )	1.8×10 <sup>19</sup>	1.8×10 <sup>19</sup>	2.2×10 <sup>17</sup>	1.1×10 <sup>18</sup>	2.2×10 <sup>18</sup>	4.8×10 <sup>15</sup>
VB effective density of states	N <sub>V</sub> (cm <sup>-3</sup> )	2.4×10 <sup>18</sup>	2.4×10 <sup>18</sup>	1.8×10 <sup>19</sup>	1.1×10 <sup>19</sup>	1.8×10 <sup>19</sup>	3.2×10 <sup>15</sup>
Electron thermal velocity	V <sub>n</sub> (cm/s)	1.0 × 10 <sup>7</sup>	1.0 × 10 <sup>7</sup>	1.0 × 10 <sup>7</sup>	1.0 × 10 <sup>7</sup>	1.0 × 10 <sup>7</sup>	1.0 × 10 <sup>7</sup>
Hole thermal velocity	V <sub>p</sub> (cm/s)	1.0 × 10 <sup>7</sup>	1.0 × 10 <sup>7</sup>	1.0 × 10 <sup>7</sup>	1.0 × 10 <sup>7</sup>	1.0 × 10 <sup>7</sup>	1.0 × 10 <sup>7</sup>
Electron mobility	μ <sub>n</sub> (cm <sup>2</sup> /v.s)	100	100	100	330	1.26	900
Hole mobility	μ <sub>p</sub> (cm <sup>2</sup> /v.s)	25	25	25	80	34.5	40
Shallow uniform donor density	N <sub>D</sub> (1/cm <sup>3</sup> )	1.0×10 <sup>17</sup>	1.0×10 <sup>21</sup>	1.0×10 <sup>22</sup>	1.0×10 <sup>17</sup>	1.0×10 <sup>17</sup>	1.0×10 <sup>21</sup>
Shallow uniform acceptor density	N <sub>A</sub> (1/cm <sup>3</sup> )	0	0	0	0	0	0

**Table 8:** the outcomes of applying the adjustment layer

	Cells	V(v)	J(mA/cm <sup>2</sup> )	FF%	η%
1.	<b><u>ZnO/ZnS/ TiO<sub>2</sub>/CNTS</u></b>	<b><u>1.040</u></b>	<b><u>19.347</u></b>	<b><u>69.91</u></b>	<b><u>14.08</u></b>
2.	ZnO/ZnS/ CdS/CNTS	1.07	17.814	69.28	12.68
3.	ZnO/ZnS/In <sub>2</sub> S <sub>3</sub> /CNTS	0.986	17.954	69.87	12.37
4.	ZnO/ZnS/ZnSe/CNTS	2.22	18.9	32.8	13.87
5.	ZnO/ZnS/SnO <sub>2</sub> /CNTS	1.319	18.02	57.23	13.61
6.	<b><u>ZnO/ZnS/V<sub>2</sub>O<sub>5</sub>/CNTS</u></b>	<b><u>1.067</u></b>	<b><u>19.349</u></b>	<b><u>69.01</u></b>	<b><u>14.25</u></b>
7.	ZnO/ZnS/SiC/CNTS	1.23	17.906	62.44	13.77

### 3.4.Results of the Best Buffer and Reflection Layers

Because TiO<sub>2</sub> has a relatively large energy gap ( 3.2 eV ), which leads to high efficiency, and the compound V<sub>2</sub>O<sub>5</sub> has little mobility, which leads to an increase in the electric field and an increase in the number of photons absorbed, the two best buffer layers (TiO<sub>2</sub>, V<sub>2</sub>O<sub>5</sub>) are studied with all of the reflection layers. It is observed that the best reflection layers with the matching layer TiO<sub>2</sub> are (MASnI<sub>3</sub>, CZTS, and SnS), while the best reflection layers with V<sub>2</sub>O<sub>5</sub> are (CFTS, MASnI<sub>3</sub>, CNTS), as indicated in Tables (9 and 10). Table (11) compares the experimental cell to the cell after improvement and cell parameters by adding the best back-reflecting Cu<sub>2</sub>O layer, then the best cell after adding a V<sub>2</sub>O<sub>5</sub> buffer layer, and finally the best cell after adding a CFTS back-reflective layer and a buffer V<sub>2</sub>O<sub>5</sub> layer.

**Table 9:** the characteristics of a solar cell after adding the reflection layers and a TiO<sub>2</sub> buffer layer

	cells	V(v)	J(mA/cm <sup>2</sup> )	FF%	η%
1.	ZnO/ZnS/TiO <sub>2</sub> /CNTS/CZTSSe	1.2	19.161	63.42	14.6
2.	<b><u>ZnO/ZnS/TiO<sub>2</sub>/CNTS/SnS</u></b>	<b><u>1.1.06</u></b>	<b><u>20.367</u></b>	<b><u>66.55</u></b>	<b><u>15.65</u></b>
3.	<b><u>ZnO/ZnS/TiO<sub>2</sub>/CNTS/MASnI<sub>3</sub></u></b>	<b><u>1.268</u></b>	<b><u>20.934</u></b>	<b><u>61.44</u></b>	<b><u>16.31</u></b>
4.	ZnO/ZnS/TiO <sub>2</sub> /CNTS/MoSe <sub>2</sub>	0.945	20.886	57.13	11.28
5.	ZnO/ZnS/TiO <sub>2</sub> /CNTS/CdTe	1.014	20.908	67.65	14.35
6.	ZnO/ZnS/TiO <sub>2</sub> /CNTS/Si	1.016	20.89	65.24	13.86
7.	ZnO/ZnS/TiO <sub>2</sub> /CNTS/ZnTe	1.043	20.08	56.22	12.26
8.	ZnO/ZnS/TiO <sub>2</sub> /CNTS/Cu <sub>2</sub> O	9.18	20.9	9.13	17.53
9.	ZnO/ZnS/TiO <sub>2</sub> /CNTS/CuO	2.09	20.909	39.69	17.01
10.	ZnO/ZnS/TiO <sub>2</sub> /CNTS/CuSbS <sub>2</sub>	0.8	20.908	57.12	9.55
11.	ZnO/ZnS/TiO <sub>2</sub> /CNTS/MoS <sub>2</sub>	1.021	20.919	59.16	12.64
12.	ZnO/ZnS/TiO <sub>2</sub> /CNTS/CISE	0.879	20.886	61.35	11.27
13.	ZnO/ZnS/TiO <sub>2</sub> /CNTS/CIGS	1.034	20.9	69.18	14.96
14.	ZnO/ZnS/TiO <sub>2</sub> /CNTS/CZTS	0.843	20.908	58.87	10.39
15.	ZnO/ZnS/TiO <sub>2</sub> /CNTS/CZTSSe	1.033	23.451	63.17	15.31
16.	ZnO/ZnS/TiO <sub>2</sub> /CNTS/CFTS	1.044	23.45	62.49	15.31
17.	ZnO/ZnS/TiO <sub>2</sub> /CNTS/CNTS	1.025	20.912	69.97	15
18.	ZnO/ZnS/TiO <sub>2</sub> /CNTS/CBTS	1.02	20.911	58.92	12.57
19.	<b><u>ZnO/ZnS/TiO<sub>2</sub>/CNTS/CZTSe</u></b>	<b><u>1.137</u></b>	<b><u>20.907</u></b>	<b><u>67.0</u></b>	<b><u>15.93</u></b>

**Table 10:** the properties of the solar cell after adding the reflection layers and the V<sub>2</sub>O<sub>5</sub> buffer layer

	Cells	V(v)	J(mA/cm <sup>2</sup> )	FF%	η%
1	ZnO/ZnS/V <sub>2</sub> O <sub>5</sub> /CNTS/Cu <sub>2</sub> Te	1.288	19.514	60.28	15.15
2	ZnO/ZnS/V <sub>2</sub> O <sub>5</sub> /CNTS/SnS	1.261	19.345	61.33	14.97
3	ZnO/ZnS/V <sub>2</sub> O <sub>5</sub> /CNTS/Si	1.242	19.205	62.11	14.82
4	ZnO/ZnS/V <sub>2</sub> O <sub>5</sub> /CNTS/CdTe	1.93	20.919	66.09	15.11
5	ZnO/ZnS/V <sub>2</sub> O <sub>5</sub> /CNTS/MoSe <sub>2</sub>	1.98	19.16	36.47	13.84
6	ZnO/ZnS/V <sub>2</sub> O <sub>5</sub> /CNTS/ZnTe	0.971	20.63	45.53	9.13
7	ZnO/ZnS/V <sub>2</sub> O <sub>5</sub> /CNTS/Cu <sub>2</sub> O	9.26	20.923	9.04	17.54
8	ZnO/ZnS/V <sub>2</sub> O <sub>5</sub> /CNTS/CuO	1.154	19.77	66.07	15.08
9	ZnO/ZnS/V <sub>2</sub> O <sub>5</sub> /CNTS/CuSb <sub>2</sub>	0.844	18.909	63.22	10.10
10	ZnO/ZnS/V <sub>2</sub> O <sub>5</sub> /CNTS/MoS <sub>2</sub>	1.027	19.769	69.62	14.13
11	ZnO/ZnS/V <sub>2</sub> O <sub>5</sub> /CNTS/CISE	0.924	19.94	62.46	11.51
12	ZnO/ZnS/V <sub>2</sub> O <sub>5</sub> /CNTS/CIGS	1.166	19.173	65.45	14.63
13	<b><u>ZnO/ZnS/V<sub>2</sub>O<sub>5</sub>/CNTS/MASnI<sub>3</sub></u></b>	<b><u>1.274</u></b>	<b><u>20.926</u></b>	<b><u>61.05</u></b>	<b><u>16.28</u></b>
14	ZnO/ZnS/V <sub>2</sub> O <sub>5</sub> /CNTS/CZTS	0.923	20.871	62.87	12.11
15	ZnO/ZnS/V <sub>2</sub> O <sub>5</sub> /CNTS/CZTSe	1.153	19.223	65.91	14.59
16	<b><u>ZnO/ZnS/V<sub>2</sub>O<sub>5</sub>/CNTS/CFTS</u></b>	<b><u>1.0937</u></b>	<b><u>23.247</u></b>	<b><u>67.74</u></b>	<b><u>17.22</u></b>
17	<b><u>ZnO/ZnS/V<sub>2</sub>O<sub>5</sub>/CNTS/CNTS</u></b>	<b><u>1.296</u></b>	<b><u>20.775</u></b>	<b><u>60.16</u></b>	<b><u>16.2</u></b>
18	ZnO/ZnS/V <sub>2</sub> O <sub>5</sub> /CNTS/CBTS	1.218	19.355	63.01	14.86
19	ZnO/ZnS/V <sub>2</sub> O <sub>5</sub> /CNTS/CZTSSe	1.211	19.22	63.3	14.74

### 3.5. Investigating the Attributes of the Best-Performing Cells

#### 3.5.1. Comparing the (V-I) Curve's Properties

The settings of each cell are entered into the SCAPS software to investigate the attributes of a current-voltage curve. The comparison between the cells shown in Table (11) reveals how to enhance the efficiency of the solar cell. Figure (4) depicts the voltage-current relationship for all cells in Table (11).

**Table 11:** the best results obtained from the study

	cells	V (v)	J (mA/cm <sup>2</sup> )	FF%	η%
1.	ZnO/ZnS/CNTS (Theoretical)	0.7359	6.743	64.26	3.19
2.	ZnO/ZnS/CNTS (After optimization)	0.934	16.749	60.11	9.41
3.	ZnO/ZnS/CNTS/Cu <sub>2</sub> O (BSL)	1.106	17.03	61.5	11.59
4.	ZnO/ZnS/V <sub>2</sub> O <sub>5</sub> /CNTS (Buffer)	1.067	19.349	69.01	14.25
5.	ZnO/ZnS/V <sub>2</sub> O <sub>5</sub> /CNTS/CFTS	1.0937	23.247	67.74	17.22

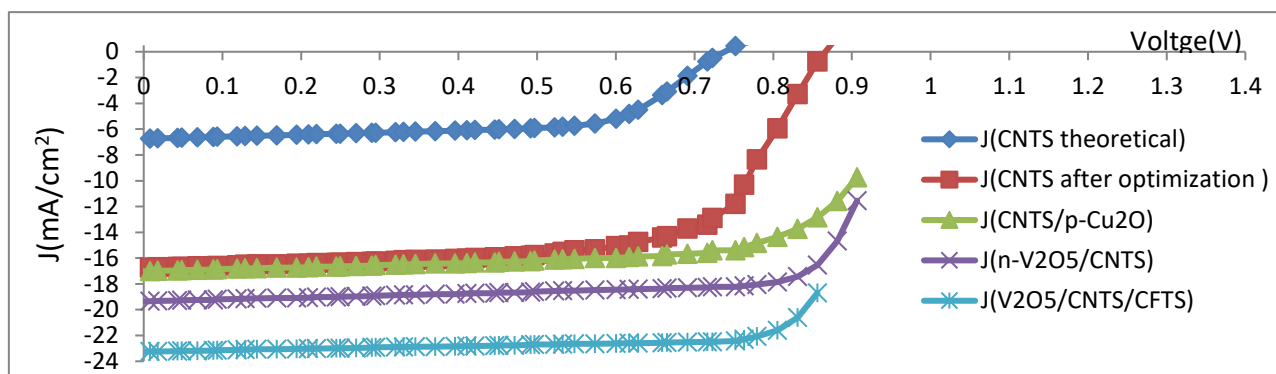


Figure 4: the voltage-current relationship for multiple cells

#### 3.5.2. Energy Plan

Figure (5) clarifies the states of the energy level. Figure (5a) shows the states of the conduction band and the valence band with the Fermi level of electrons and gaps. we note the gradation of the access layer and compatibility because the electronic affinity and energy gap for both layers are close. There is a rise between the absorption layer and the buffer layer in the conduction beam due to the difference in affinity and the energy gap between them, as shown in Table (1). As a result, a rise in the barrier voltage will be generated between the two contacting layers, which varies depending on the type of the two layers and their parameters. So, the positive conduction beam displacement will be (+CBO), which is the height of the absorption layer with the buffer layer, leading to an increase in the reunion. When there is a negative conduction beam displacement (-CBO), the absorption layer is located underneath the buffer layer, which enables the passage of light photons, inhibits recombination, and, to a certain extent, boosts the efficiency of the solar cell. If it surpasses it, the cell's efficiency will suffer. The mismatch of the lattice constant between the contacting layers is due to the differences in grain size and the

injection of impurities into the junction [12]. Figure (5b) shows a decrease in the conduction band and the Fermi level of electrons. The reason for this is that the electronic affinity for the absorption layer is smaller than the affinity for the buffer layer [38]. The second reason is that less doping and defects after improving the cell result in the formation of negative conduction bundle displacement (-CBO), which reduces the recombination. In Figure (5c), the addition of a back-reflection layer and the appearance of protrusions at the end of the energy diagram result in an increase in photon absorption and a decrease in the recombination of the generated electrons. Because it reflects photons and returns them to the absorption layer, the conversion efficiency is increased [6]. In Figure (5d), when the  $V_2O_5$  layer is added between the absorption and transmission layers, there is a drop in the conduction beam displacement (CBO +), which enhances the recombination as previously stated, as well as an increase in the beam displacement. The link (-CBO) between the absorption layer and the additional layer reduces the recombination and increases the efficiency of the solar cell. The energy levels arise in the last scenario, as shown in Figure (6), when the cell is joined to a reflection layer and a buffer layer ZnO/ZnS/ $V_2O_5$ /CNST/CFST. Due to the affinity and energy gap, a drop will emerge between ZnS/ $V_2O_5$ , resulting in an increase in the recombination and a decrease in the efficiency as previously described [39]. In addition, there is an increase in the ratio of  $V_2O_5$  / CNST, which leads to an improvement in the efficiency due to a decrease in the recombination. Moreover, there is a rise at the end of the energy diagram between the two layers CNTS / CFTS to increase the number of photons returning to the absorption layer as a result of the back-reflection layer, which boosts the conversion efficiency since the photons return to the absorption layer. The absorption layer promotes the creation of electron-hole pairs.

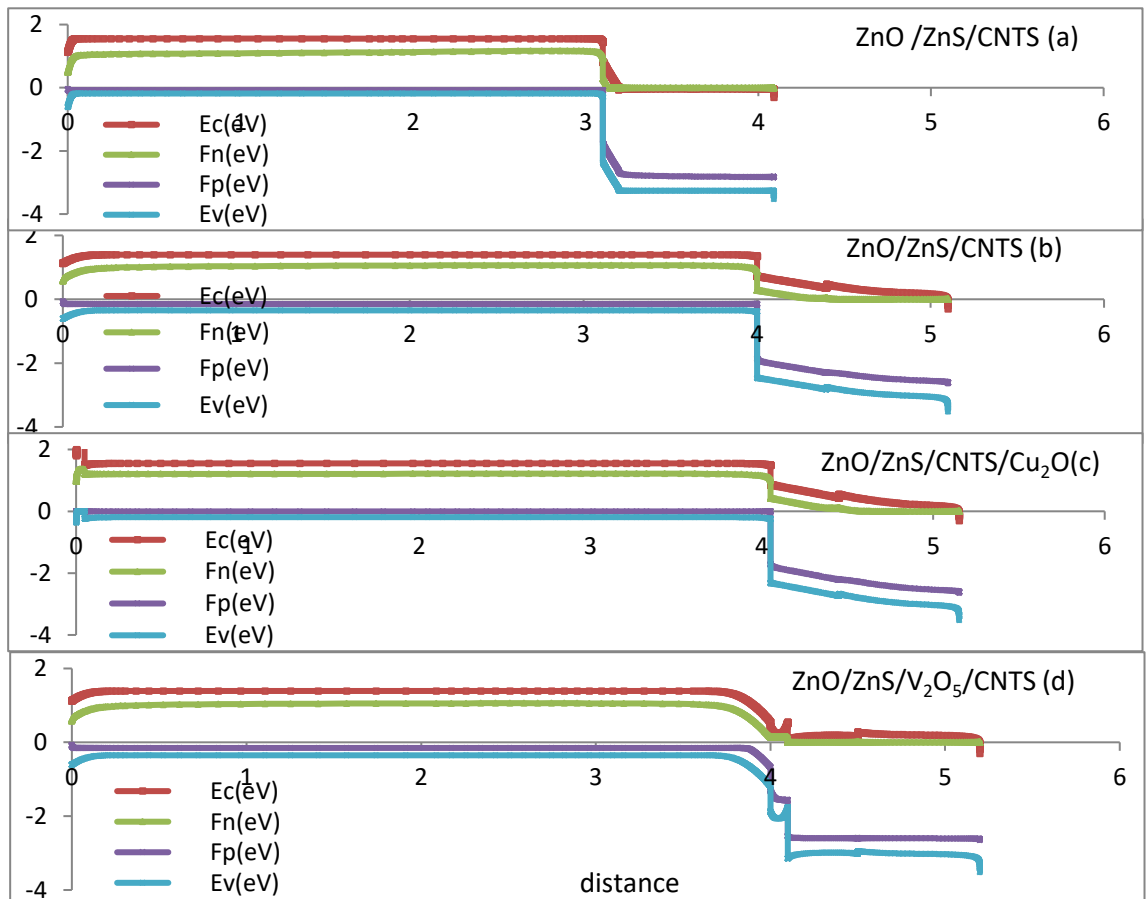


Figure 5:(a) Energy diagram of the theoretical cell; (b) The improved cell; (c) The enhanced cell following the addition of a reflection layer; and (d) The enhanced cell following the addition of a buffer layer

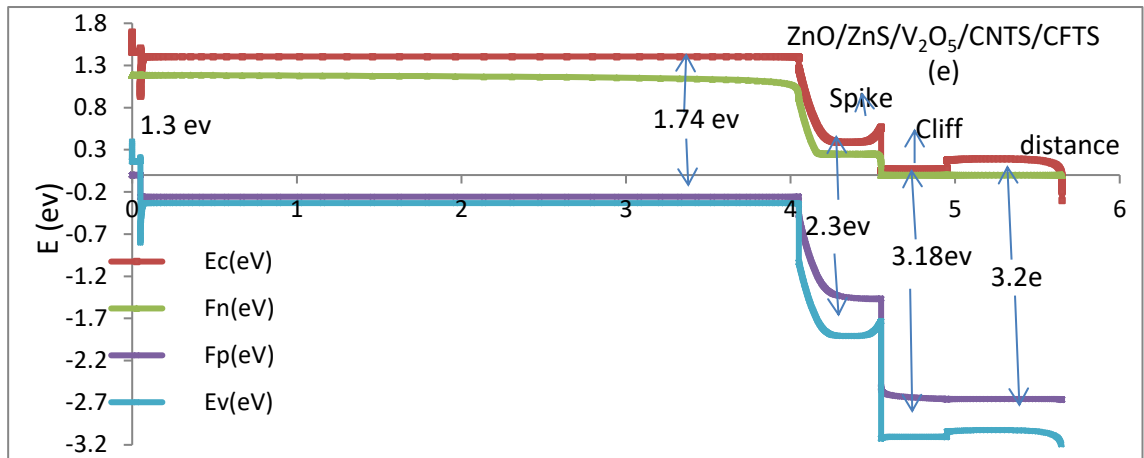


Figure 6: The enhanced cell after adding the reflection and buffer layers.

### 3.5.3. The Quantitative Efficiency

Figure (7) depicts the quantitative efficiency of the best cells and their connection to wavelength. The theoretical cell obtained from the simulation is the initial cell. It is observed that the quantitative efficiency ranges from around (95%) at wavelengths (300nm) to (400nm). Because the absorption coefficient at short wavelengths is high, absorption occurs close to the surface because the recombination period is short, resulting in the produced carriers recombining before being trapped at the junction PN [40]. Then, it begins with a sudden fall until the quantum efficiency hits (50%), due to a decrease in the absorption coefficient, which promotes the recombination, causing the quantum efficiency to decrease, and then a slow decrease begins until it approaches zero (710nm). The survivability of the carriers is improved by decreasing structural flaws, improving the durability factor, and enhancing the absorption inside the depletion area. The absorption coefficient is wavelength dependent [14]. The second cell, after improvement, has a quantitative efficiency of (100%) at

(300nm) until it reaches (375nm), which is due to a large diffusion length as it absorbs deeply, then gradually decreases until it reaches (690nm), which is due to a decrease in diffusion length and reflectivity [41]. The quantum efficiency is inversely proportional to the wavelength; hence, the efficiency is zero at (720nm) from the relationship  $Q_E = 1.24 \frac{R\lambda}{\lambda}$  [34]. The third case occurs when adding a (BSL) layer is similar to the second case. The fourth case occurs when there is a buffer layer, the quantum efficiency is (100%) at (300nm). Then, it begins with a slight gradual decrease until it reaches (690nm) and the quantum efficiency is (79%). After that, it begins with a very sharp decrease and it becomes Zero at (720nm) and sharp at the cut-off wavelength, as indicated by the following equation:  $\lambda = \frac{1.24}{E_g}$ , because the light with less energy than the gap cannot stimulate an electron from the valence band to the conduction band. In the fifth case, when there are two reflective and matching layers, the quantum efficiency is (100%) from (300nm) to (660nm) and then begins to decline sharply until (705nm). Then, the efficiency is (91%), with a rapid fall, and

the quantum efficiency is (20%) at the wavelength (720 nm). After that, there is a

steady reduction, and the quantum efficiency is (10%) at (900 nm).

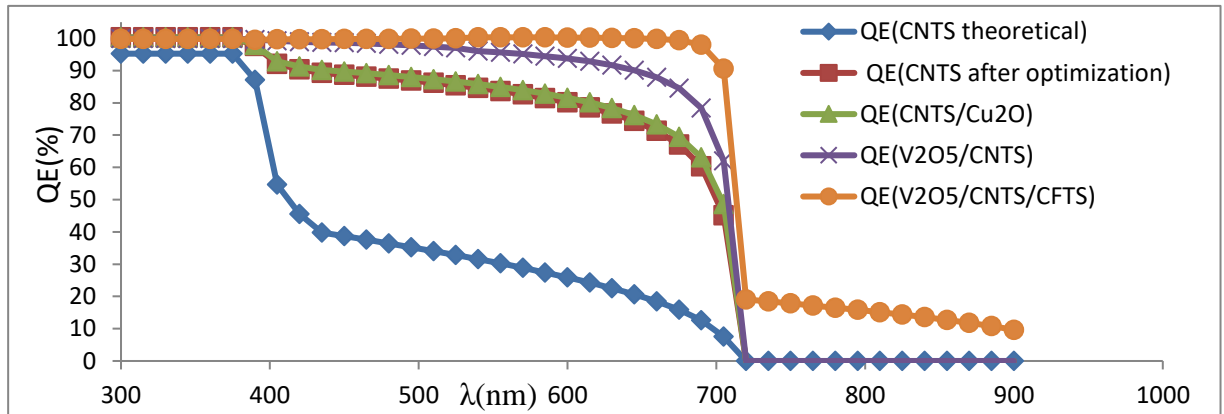


Figure 7: the quantum efficiency of the best-researched cells as a function of wavelength.

#### 4. Conclusions

There is a significant congruence between theoretical (simulation) and actual findings, which improves the program's applicability in solar cells. The direct influence of doping ratios, thickness, and crystalline flaws on cell performance is observed because lowering the percentage of doping and defects, and increasing the absorption improve the cell efficiency by reducing the electron capture-gap. Adding a back-reflection layer improves the cell efficiency by reducing the recombination. Adding a buffer layer improves the cell efficiency even more than adding a reflection layer since it leads to homogeneity between the absorption and window layers. This study reveals that the best cell is ZnO/ZnS/V<sub>2</sub>O<sub>5</sub>/CNTS/CFTS and the efficient conversion ratio is (17.22%).

#### References

[1] Skhouni, O., El Manouni, A., Bayad, H., & Mari, B. (2017). Boosting the performance of solar cells with intermediate band Absorbers the case of ZnTe: O. *Journal of Energy and Power Engineering*, 11, 417-426. Doi: 10.17265/1934-8975/2017.06.007.  
[2] Simya, O. K., Selvam, M., Karthik, A., & Rajendran, V. (2014). Dye-sensitized

solar cells based on visible-light-active TiO<sub>2</sub> heterojunction nanoparticles. *Synthetic metals*, 188, 124-129.

doi.org/10.1016/j.synthmet.2013.12.005.

[3] Sarkar, S., Howli, P., Ghorai, U. K., Das, B., Samanta, M., Das, N. S., & Chattopadhyay, K. K. (2018). Flower-like Cu<sub>2</sub>NiSnS<sub>4</sub> microspheres for application as electrodes of asymmetric supercapacitors endowed with high energy density. *CrystEngComm*, 20(10), 1443-1454. <https://doi.org/10.1039/C7CE02101A>.

[4] Khattak, Y. H., Baig, F., Ullah, S., Marí, B., Beg, S., & Khan, K. (2018). Effect of Cu<sub>2</sub>O hole transport layer and improved minority carrier lifetime on the efficiency enhancement of Cu<sub>2</sub>NiSnS<sub>4</sub> based experimental solar cell. *Journal of Renewable and Sustainable Energy*, 10(4), 043502. doi 10.1063/1.5037471.

[5] Chihi, A., Boujmil, M. F., & Bessais, B. (2019). Synthesis and characterization of photoactive material Cu<sub>2</sub>NiSnS<sub>4</sub> thin films. *Journal of Materials Science: Materials in Electronics*, 30, 3338-3348. doi: 10.1007/s10854-018-00607-z.

[6] Mokurala, K., Mallick, S., Bhargava, P., Siol, S., Klein, T. R., & Van Hest, M. F. (2017). Influence of dipping cycles on physical, optical, and electrical properties of Cu<sub>2</sub>NiSnS<sub>4</sub>: direct solution dip coating for photovoltaic applications. *Journal of*

- Alloys and Compounds*, 725, 510-518. doi 10.1016/j.jallcom.2017.07.188.
- [7] Wang, T. X., Li, Y. G., Liu, H. R., Li, H., & Chen, S. X. (2014). Flower-like Cu<sub>2</sub>NiSnS<sub>4</sub> nanoparticles synthesized by a facile solvothermal method. *Materials Letters*, 124, 148-150. doi.org/10.1016/j.matlet.2014.03.044
- [8] Beraich, M., Taibi, M., Guenbour, A., Zarrouk, A., Bellaouchou, A., & Fahoume, M. (2020). Synthesis of Tetragonal Cu<sub>2</sub>NiSnS<sub>4</sub> Thin Film via Low-Cost Electrodeposition Method: Effect of Ni<sup>2+</sup> Molarity. *Journal of Electronic Materials*, 49, 728-735. <https://doi.org/10.1007/s11664-019-07707-4>.
- [9] Skhouni, O., El Manouni, A., Mari, B. and Ullah, H., (2016). Numerical study of the influence of ZnTe thickness on CdS/ZnTe solar cell performance. *The European Physical Journal Applied Physics*, 74(2), p.24602. doi : 10.1051/epjap/2015150365.
- [10] Hameed, K.Y., Faisal, B., Hanae, T., Mari, S.B., Saira, B. and Kaim, K.N.A., (2019). Modeling of novel-structured copper barium tin sulphide thin film solar cells. *Bulletin of Materials Science*, 42(5), p.231. doi.org/10.1007/s12034-019-1919-9.
- [11] Ganvir, R., (2016). Modelling of the nanowire CdS-CdTe device design for enhanced quantum efficiency in Window-absorber type solar cells. The University of Kentucky. doi.org/10.13023/ETD.2016.036.
- [12] Baig, F. (2019). Numerical analysis for efficiency enhancement of thin film solar cells (Doctoral dissertation, Universitat Politècnica de València). DOI:10.4995/Thsis/10251/118801.
- [13] Michaelson, H.B., (1977). The work function of the elements and its periodicity. *Journal of applied physics*, 48(11), pp.4729-4733. doi 10.1063/1.323539.
- [14] Khattak, Y.H., Baig, F., Toura, H., Ullah, S., Mari, B., Beg, S. and Ullah, H., (2018). Effect of CZTSe BSF and minority carrier lifetime on the efficiency enhancement of CZTS kesterite solar cell. *Current Applied Physics*, 18(6), pp.633-641. doi 10.1016/j.cap.2018.03.013.
- [15] Ghosh, A., Chaudhary, D.K., Biswas, A., Thangavel, R. and Udayabhanu, G., (2016). Solution-processed Cu<sub>2</sub>XSnS<sub>4</sub> (X= Fe, Co, Ni) photo-electrochemical and thin film solar cells on vertically grown ZnO nanorod arrays. *RSC Advances*, 6(116), pp.115204-115212. doi : 10.1039/c6ra24149b .
- [16] Cherouana, A. and Labbani, R., (2017). Study of CZTS and CZTSSe solar cells for buffer layers selection. *Applied Surface Science*, 424, pp.251-255. <https://doi.org/10.1016/j.apsusc.2017.05.027>.
- [17] Jhuma, F. A., Shaily, M. Z., & Rashid, M. J. (2019). Towards high-efficiency CZTS solar cell through buffer layer optimization. *Materials for Renewable and Sustainable Energy*, 8, 1-7. <https://doi.org/10.1007/s40243-019-0144-1>.
- [18] Khattak, Y.H., Baig, F., Toura, H., Beg, S. and Soucase, B.M., (2019). CZTSe Kesterite as an Alternative Hole Transport Layer for MASnI<sub>3</sub> Perovskite Solar Cells. *Journal of Electronic Materials*, 48(9), pp.5723-5733. <https://doi.org/10.1007/s11664-019-07374-5>.
- [19] Khattak, Y. H., Baig, F., Soucase, B. M., Beg, S., Gillani, S. R., & Ahmed, S. (2018). Efficiency enhancement of novel CNTS/ZnS/Zn (O, S) thin film solar cell. *Optik*, 171, 453-462. doi.org/10.1016/j.ijleo.2018.06.001.
- [20] Martin A. Crane translation by Dr. Youssef Mawloud Hassan. (1989). *Solar Cells Principles of Work, Technology and System Applications*. Baghdad National Library. (in Arabic)
- [21] Mebarkia, C., Dib, D., Zerfaoui, H. and Belghit, R., (2016). Energy efficiency of a photovoltaic cell based thin films CZTS by SCAPS. *Journal of Fundamental and Applied Sciences*, 8(2), pp.363-371. doi

- 10.4314/jfas.v8i2.13.
- [22] Minbashi, M., Omrani, M. K., Memarian, N., & Kim, D. H. (2017). Comparison of theoretical and experimental results for band-gap-graded CZTSSe solar cell. *Current Applied Physics*, 17(10), 1238-1243.  
doi.org/10.1016/j.cap.2017.06.003.
- [23] Omrani, M. K., Minbashi, M., Memarian, N., & Kim, D. H. (2018). Improve the performance of CZTSSe solar cells by applying a SnS BSF layer. *Solid-State Electronics*, 141, 50-57.  
doi.org/10.1016/j.sse.2017.12.004.
- [24] Anuforonini, G. and Duduyemi, O., (2016). Simulation of the performance of CdTe/CdS/ZnO multi-junction thin film solar cell. *Simulation*, 3(1), pp.1-10. DOI:10.18488/journal.79/2016.3.1/79.1.1.10.
- [25] Boumaour, M., Sali, S., Kermadi, S., Zougar, L., Bahfir, A. and Chaieb, Z., (2019). High efficiency silicon solar cells with back ZnTe layer hosting IPV effect: a numerical case study. *Journal of Taibah University for Science*, 13(1), pp.696-703.  
<https://doi.org/10.1080/16583655.2019.1623476>.
- [26] Bayad, H., El Manouni, A., Marí, B., Khattak, Y.H., Ullah, S. and Baig, F., (2018). Influence of P+-ZnTe back surface contact on photovoltaic performance of ZnTe based solar cells. *Optical and Quantum Electronics*, 50(6), p.259. <https://doi.org/10.1007/s11082-018-1530-0>.
- [27] Sawicka-Chudy, P., Sibiński, M., Wisz, G., Rybak-Wilusz, E. and Cholewa, M., (2018), Numerical analysis and optimization of Cu<sub>2</sub>O/TiO<sub>2</sub>, CuO/TiO<sub>2</sub>, heterojunction solar cells using SCAPS. In *Journal of Physics: Conference Series* (Vol. 1033, No. 1, p. 012002). IOP Publishing. Dio.10.1088/1742-6596/1033/1/012002.
- [28] Olopade, M., Adewoyin, A., Chendo, M. and Bolaji, A., (2017), June. The Study of Some Materials as Buffer Layer in Copper Antimony Sulphide (CUSbS<sub>2</sub>) Solar Cell Using SCAPS 1-D. In *2017 IEEE 44<sup>th</sup> Photovoltaic Specialist Conference (PVSC)* (pp. 2381-2384). IEEE. doi: [10.1109/PVSC.2017.8366580](https://doi.org/10.1109/PVSC.2017.8366580)
- [29] Rafee Mahbub, M., Islam, S., Anwar, F., Satter, S. S., & Ullah, S. M. (2016). Simulation of CZTS thin film solar cell for different buffer layers for high efficiency performance. *South Asian Journal of Engineering and Technology*, 2(52), 1-10.
- [30] Nichterwitz, M., Caballero, R., Kaufmann, C. A., Schock, H. W., & Unold, T. (2013). Generation-dependent charge carrier transport in Cu (In, Ga) Se<sub>2</sub>/CdS/ZnO thin-film solar cells. *Journal of Applied Physics*, 113(4), 044515. doi.org/10.1063/1.4788827
- [31] Löckinger, J., Nishiwaki, S., Weiss, T. P., Bissig, B., Romanyuk, Y. E., Buecheler, S., & Tiwari, A. N. (2018). TiO<sub>2</sub> as intermediate buffer layer in Cu (In, Ga) Se<sub>2</sub> solar cells. *Solar Energy Materials and Solar Cells*, 174, 397-404. doi.org/10.1016/j.solmat.2017.09.030.
- [32] Khattak, Y. H., Baig, F., Ullah, S., Marí, B., Beg, S., & Ullah, H. (2018). Enhancement of the conversion efficiency of thin film kesterite solar cell. *Journal of renewable and sustainable energy*, 10(3), 033501. doi.org/10.1063/1.5023478.
- [33] Khattak, Y. H., Baig, F., Ullah, S., Marí, B., Beg, S., & Ullah, H. (2018). Numerical modeling baseline for high efficiency (Cu<sub>2</sub>FeSnS<sub>4</sub>) CFTS based thin film kesterite solar cell. *Optik*, 164, 547-555. doi.org/10.1016/j.ijleo.2018.03.055.
- [34] Hameed, K. Y., Faisal, B., Hanae, T., Marí, S. B., Saira, B., & Kaim, K. N. A. (2019). Modelling of novel-structured copper barium tin sulphide thin film solar cells. *Bulletin of Materials Science*, 42, 1-8. doi.org/10.1007/s12034-019-1919-9
- [35] Najim, A. H., & Saleh, A. N. (2019). Study effect of window and BSF layers on the properties of the CZTS/CZTSe solar cell by SCAPS-1D. *Tikrit Journal of Pure Science*, 24(3), 77-83. DOI:<https://doi.org/10.25130/tjps.v24i3.372>.
- [36] Eisele, W., Ennaoui, A., Schubert-Bischoff, P., Giersig, M., Pettenkofer, C.,

Krauser, J., ... & Karg, F. (2003). XPS, TEM and NRA investigations of Zn (Se, OH)/Zn (OH) 2 films on Cu (In, Ga)(S, Se) 2 substrates for highly efficient solar cells. *Solar energy materials and solar cells*, 75(1-2), 17-26. doi.org/10.1016/S0927-0248(02)00104-6.

[37] Zerfaoui, H., Dib, D., & Kadem, B. (2019). The simulated effects of different light intensities on the SiC-based solar cells. *Silicon*, 11(4), 1917-1923. doi.org/10.1007/s12633-018-0011-1.

[38] Gupta, G. K., & Dixit, A. (2018). Simulation studies of CZT (S, Se) single and tandem junction solar cells towards possibilities for higher efficiencies up to 22%. arXiv preprint arXiv:1801.08498.

doi.org/10.48550/arXiv.1801.08498.

[39] Bücheler, S. F. (2010). Investigation of compound semiconductors as buffer-layer in thin film solar cells (Doctoral dissertation, ETH Zurich). doi.org/10.3929/ethz-a-006246496.

[40] Mother, S. Like, the localization of both d. Fahr Ghaleb my life and d. Hussein Ali Ahmed, (1990) .*"Physics and Technology of Semiconductor Devices"*, Dar Al-Hekma for Printing and Publishing - Mosul. (in Arabic).

[41] AZZOUZI, G. (2014). Study of silicon solar cells performances using the impurity photovoltaic effect (Doctoral dissertation).